Journal of Geophysical Research: Atmospheres

RESEARCH ARTICLE
10.1002/2017JD027569

Investigation of Lightning Flash Locations in Isolated Convection Using LMA Observations

Brody R. Fuchs[1] and **Steven A. Rutledge**[1]

[1]Department of Atmospheric Science, Colorado State University, Fort Collins, CO, USA

Key Points:
- Lightning flash locations are investigated using multiple methods and collocated with reflectivity using a large database
- Anomalously electrified storms in Colorado produced flashes at lower altitudes and in higher radar reflectivities
- Lightning locations in the vertical may have implications for satellite optical detection and production efficiency of nitrogen oxides and ozone

Correspondence to:
B. R. Fuchs,
brfuchs@atmos.colostate.edu

Citation:
Fuchs, B. R., & Rutledge, S. A. (2018). Investigation of lightning flash locations in isolated convection using LMA observations. *Journal of Geophysical Research: Atmospheres*, *123*, 6158–6174. https://doi.org/10.1002/2017JD027569

Received 19 SEP 2017
Accepted 11 MAR 2018
Accepted article online 14 MAR 2018
Published online 14 JUN 2018

Abstract Using Lightning Mapping Arrays (LMAs), lightning flash locations in three dimensions have been investigated using multiple methods. Approximately 500,000 flashes were analyzed to reveal the variability of lightning initiation and propagation within convective storms. These flashes were produced by over 4,000 isolated convective storms during one warm season across diverse weather regimes in northern Alabama, Washington, D.C., central Oklahoma, and northeastern Colorado. Lightning locations are analyzed within the context of radar reflectivities and examined for vertical variability. Results show that storms in Colorado preferentially produced flashes at lower altitudes and in regions of higher reflectivity compared to the other regions. The regional differences in flash altitudes are largely attributed to the prevalence of anomalous polarity storms (middle- or low-level dominant positive charge) in Colorado, as anomalous storms produced a majority of flashes at lower altitudes compared to storms with normal polarity charge structures (middle-level negative charge). Conversely, anomalous storms are exceedingly rare in the other regions of study. The differences in flash altitudes are coincident with discrepancies between annual average densities estimated by satellite observations and LMA. Specifically, large differences in annual average flash density estimates exist in northeastern Colorado, which are not present in the other regions, suggesting that the lower altitude flashes in Colorado may be more difficult to detect by satellites.

1. Introduction

1.1. Thunderstorm Charging

Lightning is generated by microscale processes but has impacts on much larger scales. Collisions between large precipitation ice particles (graupel) and small ice crystals in the presence of supercooled cloud liquid water (SCLW) result in significant charge separation on the particle scale (e.g., Jayaratne et al., 1983; T. Takahashi, 1978; Workman & Reynolds, 1950). The sign and magnitude of charge acquired by graupel depends both on temperature and SCLW content. Specifically, regions in the cloud with higher temperatures and SCLW tend to charge graupel positively, while regions with lower temperatures and SCLW tend to charge graupel negatively (e.g., Saunders & Peck, 1998). Strong electric fields result when gravity and convective updrafts vertically separate large and small particles, separating electrical charge of opposite polarity (Williams, 1985).

Because most of the initial charging of graupel and small ice particles occurs in the mixed-phase region (~0°C to −40°C), it is hypothesized that the charge structure within a storm depends on SCLW in the mixed-phase (e.g., Bruning et al., 2014; Saunders et al., 1991; H. Takahashi et al., 2017; Williams et al., 2005). Most thunderstorms possess a normal charge structure consisting of midlevel negative charge situated between regions of upper- and lower-level positive charge (e.g., Williams, 1989). The midlevel negative charge is thought to be composed of negatively charged graupel particles, which suggests that SCLW amounts are modest. Accordingly, ice crystals acquire positive charge from collisions with midlevel graupel and are carried to the storm's upper levels. The dipole composed of the midlevel negative and upper-level positive charge regions drives intracloud (IC) flashes between these two layers, which account for most of the lightning flashes in a normal polarity storm (Boccippio et al., 2001; Krehbiel, 1986; Krehbiel et al., 1979).

1.2. Thunderstorm Charge Structure Variability

While most storms possess a normal polarity charge structure (e.g., Williams, 1989), some storms possess an "inverted" or "anomalous" (hereafter anomalous) charge structure. Anomalous charge structures are marked by a dominant middle- or low-level positive charge region, which is thought to be comprised of positively charged graupel, suggesting the presence of large SCLW contents (Fuchs et al., 2015; MacGorman et al., 2005; Rust et al., 2005; Tessendorf et al., 2007; Wiens et al., 2005). Accordingly, negatively charged ice crystals

are carried to the upper levels of these storms. The existence of a lower-level negative charge region has been hypothesized in these storms, but evidence of its existence is rather tenuous (Lang et al., 2000).

Fuchs et al. (2015) recently detailed significant variability in macroscale charge structures in isolated convective storms for one warm season using four Lightning Mapping Arrays (LMAs). In northern Alabama, Washington, D.C., and central Oklahoma, the majority of isolated convective storms possessed a normal polarity charge structure, marked by LMA-inferred dominant positive charge in the upper levels near −40°C (section 2.3). Conversely, the vast majority of isolated convective storms in northeastern Colorado possessed an anomalous charge structure, marked by LMA-inferred dominant positive charge at temperatures warmer than −25°C (section 2.3).

In an effort to understand the mechanisms that produce anomalous storms in the Colorado region, Fuchs et al. (2015) found that Colorado storms had substantially higher cloud base heights and shallower warm cloud depths, leading to their hypothesis that these parameters strongly influence the mixed-phase SCLW amounts, which in turn dictate the storm-scale charge structure. Indeed, in a more detailed comparison of several storms in Alabama and Colorado, Fuchs et al. (2018) found that anomalous polarity storms had stronger and broader updrafts than normal polarity storms. Moreover, they found that anomalous storms had more robust mixed-phase microphysics by a variety of measures, including an indication of positively charged graupel in the midlevels and high SCLW contents.

Lightning initiates in regions where the local electric field exceeds the breakdown threshold of air (Maggio et al., 2005). After initiation, lightning channels propagate through regions of charged hydrometeors with the effect of neutralizing the buildup of charge (Coleman et al., 2003; MacGorman et al., 2001). Therefore, the location of initiation and propagation of each lightning flash is dependent on the location and charge density of nearby charge regions. Therefore, it should follow that storm-integrated lightning flash locations should be related to storm-scale charge structures. Given the regional differences in storm-scale charge structures, and the controlling factors of storm-scale charge structures on flash locations, it is reasonable to expect some differences in the vertical lightning locations between the normal polarity storms in Alabama, D.C., and Oklahoma and the anomalous storms in Colorado. However, the exact nature of those details is not yet known, and investigating that is precisely one of the primary goals of this paper.

1.3. Lightning Detection by LMA and Satellite

Beyond a pure scientific interest in lightning location variability, there may be practical considerations as well. In a comparison between multiple years of satellite and ground-based LMA lightning observations, Fuchs et al. (2016) found LMA-based annual flash density estimates were $<$ 50% higher than satellite estimates in northern Alabama and D.C. These differences were considered reasonable because these observing systems use different detection techniques and observe different physical processes. Specifically, LMAs detect subflash processes in the very high frequency (VHF) portion of the electromagnetic spectrum (Rison et al., 1999), while satellite detectors use optical sensors viewing the storm from above (Christian et al., 1999, 2003). In northeastern Colorado, however, LMA-based annual flash density estimates were approximately 300% higher than corresponding satellite-based estimates, which was considered physically significant. Furthermore, the ratios of intracloud to cloud-to-ground flashes (IC:CG) in northeastern Colorado (based on LMA observations) were also approximately 300% higher than previous studies based on satellite estimates (e.g., Boccippio et al., 2001).

1.4. Lightning Production of Nitrogen-Oxides

One of the possible reasons Fuchs et al. (2016) offered for the discrepancies was flash altitude. Specifically, they showed that most flashes in the Alabama and D.C. regions initiated near 9–10 km mean sea level (MSL), while most flashes in northeast Colorado initiated near 6–7 km MSL. Note that the distributions of flash area (or size) were not substantially different in the respective regions. They hypothesized that anomalous storms in Colorado have different distributions of charge which results in a propensity for lower altitude flashes in those storms. Accordingly, these flashes are more difficult to detect because they produce photons that must propagate through a longer optical path to reach the satellite detector. However, Fuchs et al. (2016) only had access to flash initiation information and were thus unable to conclude that the full extent of lightning flash propagation in Colorado storms remained at lower altitudes. Indeed, one of the goals of the present study is to address this hypothesis by investigating the full spatial extent of lightning initiation and propagation and its variability with respect to region and storm-scale charge structure.

In addition to satellite detection considerations, lightning impacts its environment, including the production of nitrogen oxides (e.g., Schumann & Huntrieser, 2007). Heated lightning channels dissociate diatomic nitrogen and oxygen, creating NO and NO_2 molecules, collectively called NO_x (e.g., Goldenbaum & Dickerson, 1993; Huntrieser et al., 1998). Lightning-generated NO_x (LNO_x) is important in the atmosphere, especially in the upper troposphere, because it is a precursor for tropospheric ozone, an important greenhouse gas (DeCaria et al., 2005; Price et al., 1997). Schumann and Huntrieser (2007) claim that lightning is the dominant source of NO_x in the upper troposphere.

Importance has been placed on the vertical variability of lightning flash channels, since NO_x-based ozone production efficiency depends on ambient temperature, hydrocarbon concentration, NO_x concentration, and NO_x lifetime, all of which vary with altitude (Finney et al., 2016; Lin et al., 1988). Therefore, any variability in lightning locations may impact the amount of ozone produced by a particular storm. Furthermore, many chemistry models place LNO_x uniformly in the horizontal within the 20 dB*Z* isopleth (Ott et al., 2010; Pickering et al., 1998); therefore, it is important to understand lightning locations with respect to reflectivity.

1.5. Paper Overview

The substantial differences in flash initiation heights in thermodynamically and electrically distinct regions in Fuchs et al. (2015, 2016) provide significant motivation to investigate the locations of lightning initiation and propagation. Moreover, the location of lightning influences the subsequent transport of LNO_x and conversion to ozone (DeCaria et al., 2000; Pickering et al., 1998) and possibly the ability to optically detect lightning from spaceborne platforms including the current Geostationary Lightning Mapper (Fuchs et al., 2016). This study investigates lightning flash locations using multiple methods based on highly accurate LMA observations from the statistically significant data set of isolated convective storms originally crafted by Fuchs et al. (2015). Lightning locations are investigated with respect to height as well as reflectivity. Importance will be placed on regional differences of these quantities and their relationship with LMA-inferred charge structure.

2. Data and Methodology

2.1. Radar

The radar data in this study are derived from the National Mosaic and Multi-Sensor Quantitative Precipitation Estimates (NMQ) mosaic 3-D radar data set (Zhang et al., 2011). NMQ data consist of gridded reflectivity data from Next Generation Radar Weather Surveillance Radars (NEXRAD-WSR88D) covering the entire continental United States with a temporal resolution of 5 min during the observation period (2011–2012). NMQ Cartesian mosaic data provide approximately 1 km × 1 km horizontal resolution with a stretched vertical grid from 500 m to 18 km above MSL. The vertical resolution varies from 500 m near the surface to 2 km near the top of the domain.

NMQ data centered near LMAs in four environmentally distinct regions (Washington, D.C., northern Alabama, central Oklahoma, and northeast Colorado) for one warm season was used to produce a database of over 4,000 observations of isolated convective storms containing over 500,000 flashes. The data in Alabama, D.C., and Oklahoma came from the 2011 warm season, while the Colorado data came from the 2012 warm season (the Colorado LMA was installed in the spring of 2012).

2.2. CLEAR

The data set for this study was originally created by Fuchs et al. (2015) using the Colorado State University Lightning, Environmental, Aerosol and Radar (CLEAR) automated case study framework (Lang & Rutledge, 2011). CLEAR was specifically designed to make analysis on large and multifaceted datasets (such as the present one) tractable. This is accomplished by using objective cell identification and tracking on composite reflectivity fields, then attributing various types of information to identified cells, such as lightning flashes from LMA data. Strict criteria were imposed for cell identification: contiguous 35 dB*Z* regions of area $\geq$ 20 km^2 containing a contiguous 45 dB*Z* region of area $\geq$ 13 km^2 were required for a cell to be included in the analysis. This resulted in the removal of most small and nonlightning-producing cells while preserving storms near the mature phase of their lifecycle.

Each objectively identified cell for each radar volume time was treated as an independent storm sample for the purposes of statistical aggregation in this study. Additionally, storms were classified as isolated and included in the analysis as follows. Once the cells were objectively identified, the Yuter and Houze (1998)

convective-stratiform algorithm was used to identify convective regions. If a contiguous convective region only contained one objectively identified cell, that cell was classified as isolated and included in the analysis. If, however, a contiguous convective region contained multiple identified cells, those cells were classified as organized and left out of the analysis. Restricting analysis to isolated convective cells allows us to focus on more idealized storm structures and avoid complications such as cell mergers, splits, and influences from nearby convection.

2.3. LMA

LMA networks use time-of-arrival differences from multiple antennae to detect VHF radiation sources produced by the discontinuous breakdown of lightning channels (Rison et al., 1999). LMAs can accurately detect the in-cloud portion of flash channels (Krehbiel et al., 2000), making them a great candidate for the analysis methods in the present study. LMAs may detect a few VHF sources to a few thousand VHF sources from a single flash, depending on the spatial extent of the physical flash, the location of the flash relative to the network, and the detection capabilities of the network (Fuchs et al., 2016; Thomas et al., 2004). VHF source location errors are on the order of tens of meters within the physical boundary of the network and increase with distance from the center of the network (Thomas et al., 2004). Additionally, detection efficiency decreases with increasing range from the network center (Chmielewski & Bruning, 2016; Fuchs et al., 2016; Koshak et al., 2004; Thomas et al., 2004). Accordingly, only identified cells within 125 km of their respective LMA centers are included in the analysis to mitigate LMA detection efficiency and location artifacts. To further minimize location errors, only VHF sources that had seven or more stations contributing to the solution and a chi-squared goodness-of-fit parameter $\leq$1 were included in analysis. If a particular VHF source was within the volume of a valid cell, it was attributed to that cell. VHF sources that were within 10 km of the edge of valid cells were also attributed to the closest cell. Sources more than 10 km from cell edges were dismissed.

LMA detection of leader propagation depends on channel polarity (Rison et al., 1999). Once a lightning flash is initiated, leaders of opposite polarity propagate toward regions of opposite charge to neutralize charge buildup. Negative leader propagation into positive charge is more discontinuous than propagation of positive leaders into negative space charge, resulting in negative leaders producing more VHF radiation than positive leaders (Rison et al., 1999). This asymmetry has been used to infer charge polarity, both on a flash-by-flash scale and a storm scale, by inferring positive charge near the location of highest VHF source density.

On an idealized storm scale, the mode of the vertical LMA source density profile is used to infer the charge structure: normal polarity storms are typically defined as having an LMA modal temperature near -40°C and anomalous polarity storms are typically defined as having an LMA modal temperature around -20°C (Fuchs et al., 2015; Lang & Rutledge, 2011; Wiens et al., 2005). However, since LMA depictions of flashes tend to be biased toward the negative leaders (positive charge), analysis of LMA-detected flash initiation and propagation will be subject to the same bias. Implications for this are explored in sections 2.4 and 2.5.

2.4. LMA Flash Algorithm and Lightning Location Estimation

Because LMA networks detect subflash features (Bruning et al., 2007; Rison et al., 1999; Thomas et al., 2001), further processing of VHF source data is required to retrieve information about individual flashes. Bruning (2013) and Fuchs et al. (2015, 2016) described a flash-clustering algorithm that groups sources by space and time for flash identification. Because the LMA networks used in this study have different sensitivities, network-dependent thresholds were used. The Oklahoma and Colorado LMA networks have been shown to be more sensitive than the Alabama and D.C. LMA networks (Chmielewski & Bruning, 2016; Fuchs et al., 2016; Koshak et al., 2004). As such, the spatial search radius (maximum separation between nearby VHF sources to be considered in the same flash) was set at 3 km for the Oklahoma and Colorado networks while a more generous 6 km threshold was used for the Alabama and D.C. networks. The temporal search radius for all networks was set at 0.15 s. The threshold for an algorithm-identified flash to be considered in the analysis was set to 10 VHF sources in Oklahoma and Colorado and 2 VHF sources in Alabama and D.C. These search radii and source thresholds are in accordance with previous studies (e.g., Fuchs et al., 2015, 2016; McCaul et al., 2009), which have been shown to consistently produce realistic results.

Once the VHF sources are grouped into flashes, useful information about each flash, such as location and spatial extent can be extracted. Of particular interest to this study are the locations and spatial extent of flash channel propagation. Strictly speaking, VHF radiation is the direct result of discontinuous propagation of lightning flash channels, so the use of VHF sources as a metric for flash locations is physically sound.

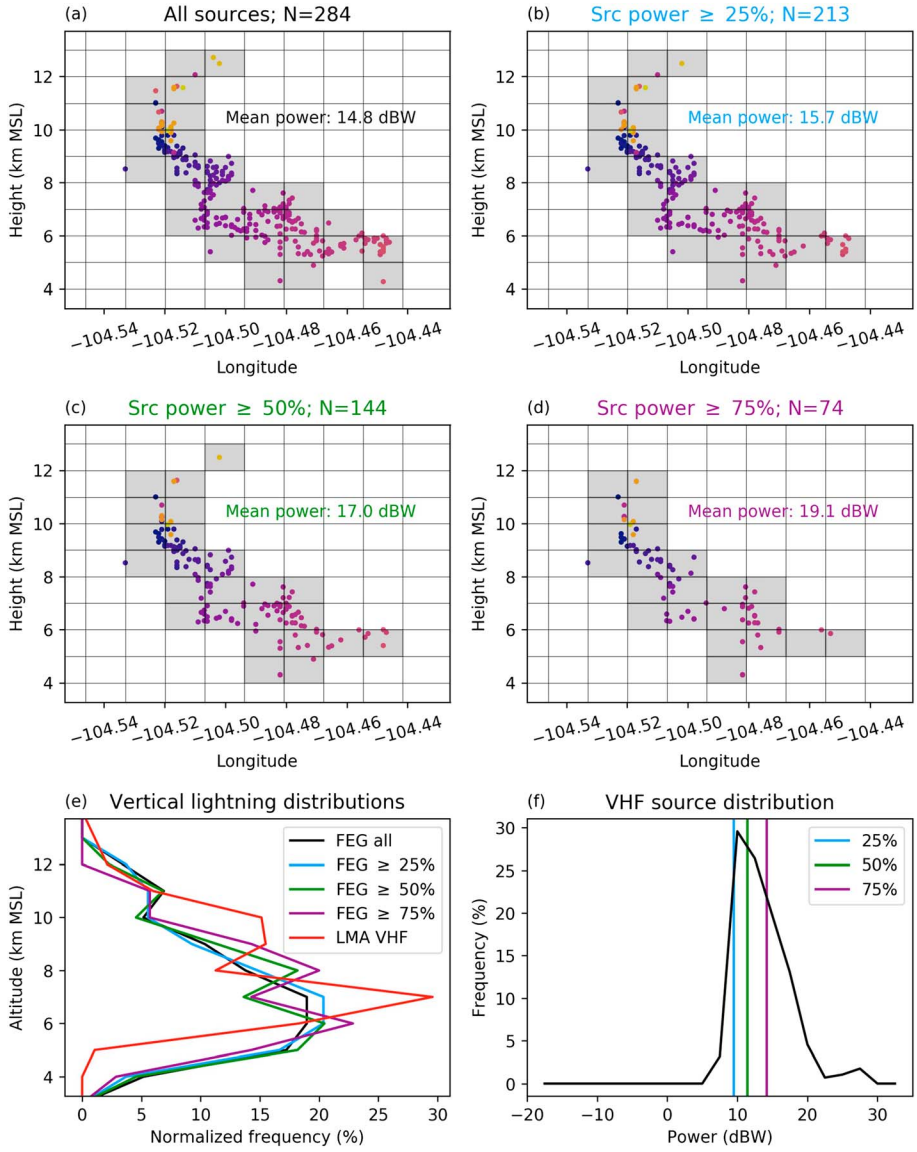

Figure 1. (a) Illustration of the flash extent grid (FEG) calculation. Points are Lightning Mapping Array (LMA) very high frequency (VHF) sources colored by time (dark purple to light yellow). Grid boxes highlighted in gray are considered to contain a segment of the flash. (b) Same as (a) but with the lowest 25% of VHF source powers removed. (c) Same as (a) but with the lowest 50% of VHF source powers removed. (d) Same as (a) but with the lowest 75% of VHF source powers removed. (e) Vertical distribution of flash extent grids from each representation of the flash in (a)–(d) and VHF source distribution. The colors follow the legend in the panel. (f) Distribution of VHF source powers (black) with the threshold powers shown in the vertical lines. The colors of the lines follow the legend in the panel. MSL = mean sea level.

However, as discussed earlier, negative channels produce more VHF radiation than positive channels. As a result, naively using VHF sources will result in biases toward positive charge.

Another method for estimating the three-dimensional spatial extent of flashes is to use the three-dimensional extension of the flash extent density approach (Mansell, 2014). This method begins by imposing a grid on the VHF sources comprising a flash. Then, any grid box containing at least one VHF source is considered to have contained a segment of that flash. Those grids are assigned a value of 1 while grids not containing a flash segment are assigned a 0. When these grids are summed for numerous flashes, over a storm volume, for example, the resulting values represent the number of flashes with LMA-detected segments that passed through a particular grid box. Figure 1 shows an illustration of both the VHF source method and the flash extent method on a longitude-altitude cross section with a 1 km grid. This flash occurred in Colorado, approximately 20 km from the

center of the Colorado LMA network, and was chosen because the high detection efficiency of the Colorado LMA (Fuchs et al., 2016). In Figure 1a, grid boxes containing VHF sources from the flash are highlighted to indicate that a segment of that flash passed through those boxes. The corresponding vertical distribution of calculated "flash extent grids" (FEG) is shown in Figure 1e, which shows most of the flash residing between 5 and 8 km MSL. In comparison to the VHF source density profile, the flash extent grid profile has less prominent peaks and is smoother than the VHF profile. This is not surprising since the flash extent method gives equal weight to each grid box containing VHF sources, regardless of the actual number of VHF sources in the grid box.

The average power of the VHF sources in the original flash is 14.9 dBW, which is typical of Colorado flashes (Fuchs et al., 2016). To simulate decreasing detection efficiency, Figure 1b shows the same flash as Figure 1a, but with the lowest 25% of VHF source powers removed. Because the power from an isotropically emitting source follows the inverse square law, weaker sources may not be detected at longer ranges. Therefore, removing low VHF source powers is analogous to moving the flash farther away from the network center. The distribution of VHF source powers for this flash is shown in Figure 1f, with the 25th, 50th, and 75th percentiles of those VHF source powers indicated by the vertical lines. The 25th percentile of VHF source powers for this flash is approximately 8 dBW. The distribution of flash extent grids in Figure 1b largely resemble the flash extent grids from the original flash in Figure 1a, except a couple of grid boxes are missing. It is important to note that the vertical distribution of calculated flash extent grids is nearly identical to the original flash (Figure 1e). Further simulated degradation of LMA source detection is shown in Figure 1c (Figure 1d), which shows only the sources that have powers greater than the 50th (75th) percentiles within the flash. As sources are removed from the flash, the depiction of the flash becomes less complete.

A key point is that the vertical distribution of calculated flash extent grids for each case Figures 1b–1d (each line in Figure 1e) closely resembles that of the original flash. Since the vertical distribution of flash extent grids is of principal interest to this study, perhaps variable detection efficiency will not lead to a substantial bias in calculated flash extent grids. To test this assertion, we removed low-power VHF sources from numerous random flashes in a manner similar to Figure 1 and found no systematic differences between vertical distributions of calculated extent grids. Note that the difference in average power from the original flash (Figure 1a) to the flash subset of the 25% highest powers (Figure 1d) is approximately 4 dBW. Results from Fuchs et al. (2016) suggest that a 4–5 dBW increase in average power is equivalent to moving the flash from inside the network to approximately 100 km from the network center.

2.5. Sensitivities

The calculation of flash extent grids requires an imposed grid upon which the flash is mapped out. Therefore, it is reasonable to expect that the calculated flash extent grids will be sensitive to the imposed grid size. Moreover, it is not immediately obvious that an optimal grid size for flash extent grids exists. Therefore, our approach was to explore the results with two different grid sizes. We chose uniform 1.0 km and 2.0 km grids since the uncertainty in VHF source location in range and height is approximately 1.0 km at 125 km range from the LMA network center (Thomas et al., 2004).

Figure 2 illustrates how the grid size may affect the resulting flash extent grids and VHF source distributions on the same flash shown in Figure 1. Figure 2a shows a time-height cross section of the flash. The first sources occur around 10 km MSL. Shortly after initiation, the heights of the sources descend to approximately 6 km MSL during the first 100 ms. Figure 2b shows the vertical distribution of VHF sources gridded to 1.0 km (red), where a maximum near 7 km MSL is evident. The gold curve in Figure 2b shows the flash extent grid product also gridded to 1.0 km. Like Figure 1, a smoother distribution with a less prominent peak is evident compared to the VHF distribution. The blue lines in Figure 2b show the vertical distribution of flash extent grids and VHF sources, gridded to 2.0 km. Obviously, the depiction of the flash becomes less well defined with the coarser grid. However, the distribution of flash extent grids remains smoother with a less prominent peak than the VHF distribution, similar to the 1.0 km grid.

3. Results

3.1. Flash Locations With Respect To Altitude and Reflectivity

This section will focus on calculated flash altitudes (VHF sources and flash extent grids) and their collocated reflectivity values (from NMQ mosaic radar data). Due to the mismatch between radar data and the imposed

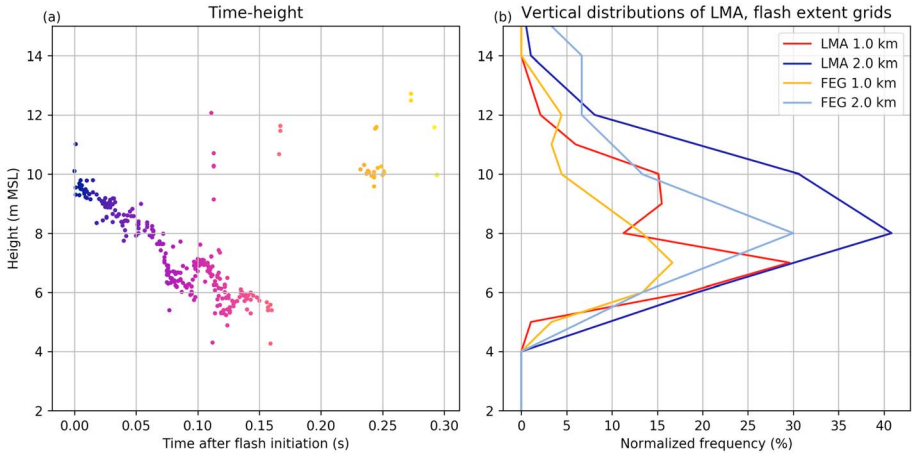

Figure 2. (a) Time-height cross section of a sample flash. Points are Lightning Mapping Array (LMA) very high frequency sources colored by time (dark purple to light yellow). (b) Vertical distribution of LMA very high frequency sources gridded at 1.0 km (red) and gridded at 2.0 km (dark blue). Vertical distribution of flash extent grid (FEG) at 1.0 km (gold) and 2.0 km (light blue). MSL = mean sea level.

grids, lightning grids are matched with the reflectivity from the nearest radar grid point. Sensitivity studies (not shown) indicate little dependence on the reflectivity collocation method. For every flash in each isolated convective cell, the grids are calculated based on the imposed grid, then the height and corresponding reflectivity values are recorded and saved. All the heights and reflectivities corresponding to each channel of every flash are summed and normalized by the number of cells in each region.

The resulting distributions from the collocated VHF grids at 1.0 km are shown in Figure 3, which are effectively the climatological distributions of altitudes and collocated reflectivity values for LMA-detected flash channels. In Alabama (AL), the peak VHF source production was between 8 and 9 km MSL and the majority of the VHF sources occurred between 7 and 10 km MSL. Approximately 40% of all VHF sources occurred below 8 km. Note that the choice of 8 km is somewhat arbitrary, but the general results do not change with different height choices. The average collocated reflectivity was 24.7 dBZ and 37% of all VHF sources occurred in reflectivities $<$20 dBZ.

The VHF source distribution in the D.C. region is quite similar to the AL region, as most of the VHF sources reside between 7 and 10 km MSL. The average VHF source height is the same as in AL, while the average collocated reflectivity is slightly higher at 27.4 dBZ. Roughly one quarter of the VHF sources were situated in reflectivities below 20 dBZ. The VHF source distribution in Oklahoma (OK) is shifted downward relative to the AL and D.C. regions, with most of the VHF sources residing between 6 and 9 km MSL. Over half of all VHF sources in the OK region occurred below 8 km MSL, approximately 10% more than AL or D.C. The average collocated reflectivity is 32.9 dBZ, higher than either AL or D.C. Only a small fraction (14%) of VHF sources in Oklahoma occurred in regions with reflectivities less than 20 dBZ. These results are consistent with the Oklahoma cases being generally more intense compared to the storms observed in AL and D.C. OK storms had higher reflectivity values in the 7–10 km MSL layer compared to AL and D.C. storms (Figures 5b and 5c in Fuchs et al., 2015). The VHF source distribution in Colorado is the most bottom heavy, as most of the VHF sources were located between 4 and 8 km MSL. Three quarters of the VHF sources were produced below 8 km MSL. The average collocated reflectivity value is 36.2 dBZ, highest of any region. Only 7% of VHF sources occurred in regions of less than 20 dBZ.

Figure 4 was constructed in the same manner as Figure 3 but shows the distributions of calculated flash extent grids instead of VHF sources. Overall, Figure 4 shows similar results to Figure 3, with some small but important differences. In each region, the peak of the distribution remains approximately the same, but the distributions are broader with less prominent peaks. For instance, most flash extent grids in AL and D.C. occur between 7 and 10 km MSL, but the fraction of flash extent grids occurring below 8 km has marginally increased by about 3% in each region. In OK, the distribution is still peaked between 6 and 9 km, but the fraction of flash extent grids below 8 km is 61% compared to 56% of VHF sources. Like the other regions, the CO flash extent grid distribution is broader compared to the VHF sources but is still at a markedly lower altitude relative to the other regions.

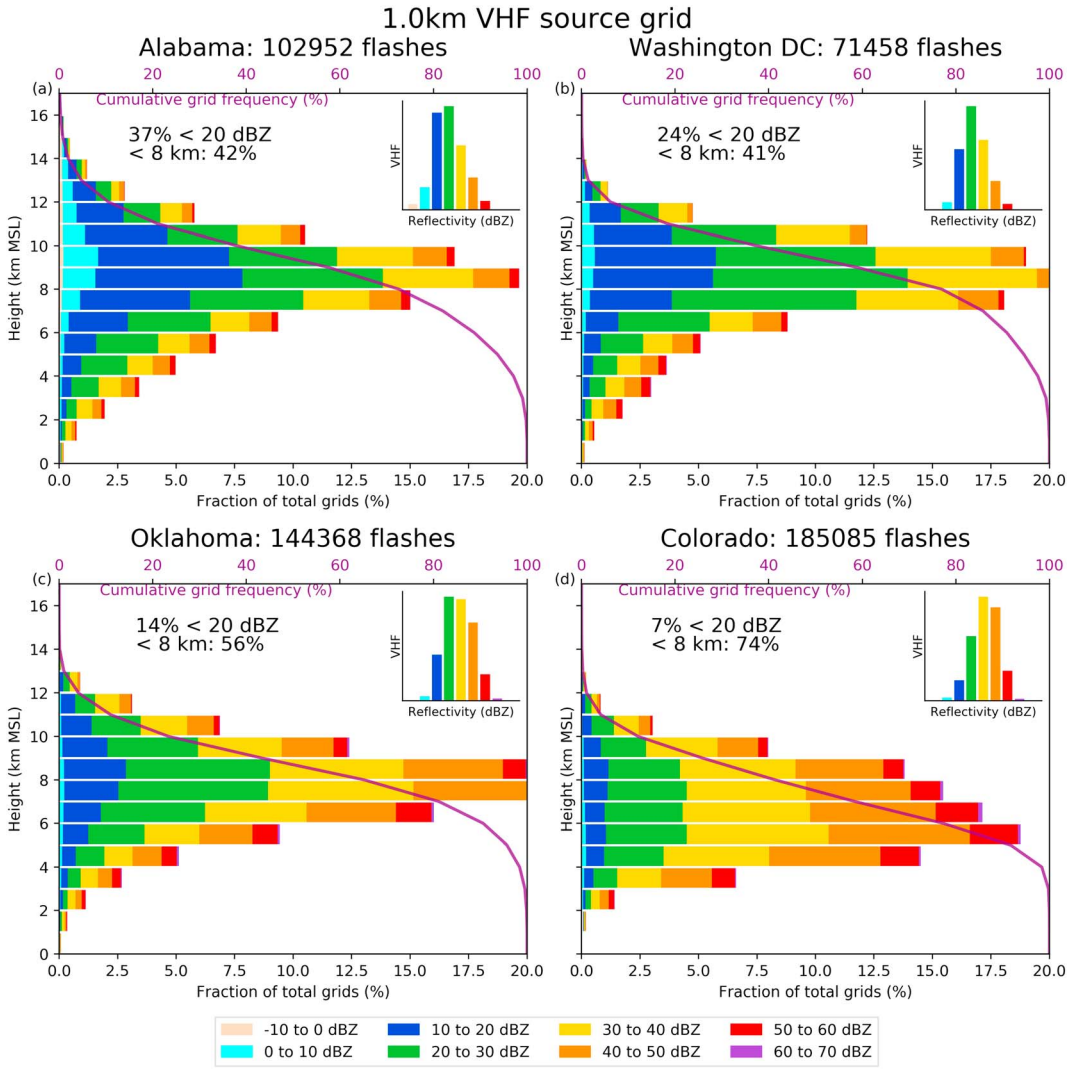

Figure 3. Collocated very high frequency (VHF) sources on a 1.0 km grid with respect to height and reflectivity for all cells in (a) Alabama, (b) Washington, D.C., (c) Oklahoma, and (d) Colorado. The inset panels show VHF source density with respect to reflectivity only. The purple line indicates the cumulative fraction of VHF sources above a particular height and follows the purple axis on the top of the panel. The average VHF source height and collocated reflectivity are shown in each panel as well as the fraction of VHF sources in regions of less than 20 dBZ and below 8 km mean sea level (MSL).

Figures 5 and 6 show the VHF source and flash extent grid distributions calculated with a 2.0 km grid, respectively. No significant differences can be found when comparing the 2.0 km grid results with the 1.0 grid results of Figures 3 and 4. The most notable difference may be the fraction of grids occurring below 8 km MSL, which are higher compared to the 1.0 km grid in each region. However, this is largely an artifact introduced by the gridding process. This coarsening of the results may suggest that the optimal grid size may be closer to 1.0 km. However, this will depend on the LMA location errors and where the lightning occurs relative to the LMA center.

Regardless of lightning metric or grid size, the distributions in the Colorado region were substantially lower in altitude and situated in higher reflectivity than the other regions, suggesting that the flashes are indeed lower in CO storms. However, as discussed earlier, both the VHF source and flash extent methods are subject to the inherent biases toward the positive charge in the LMA. Since anomalous storms are common in the Colorado region in this data set, we expect the dominant positive charge to be located at lower altitudes in Colorado storms compared to storms in other regions, which may be responsible for the altitude differences in Figures 3–6. Therefore, a method of measuring full vertical flash extent that is insensitive to LMA biases would be ideal. This idea is explored further in the next section.

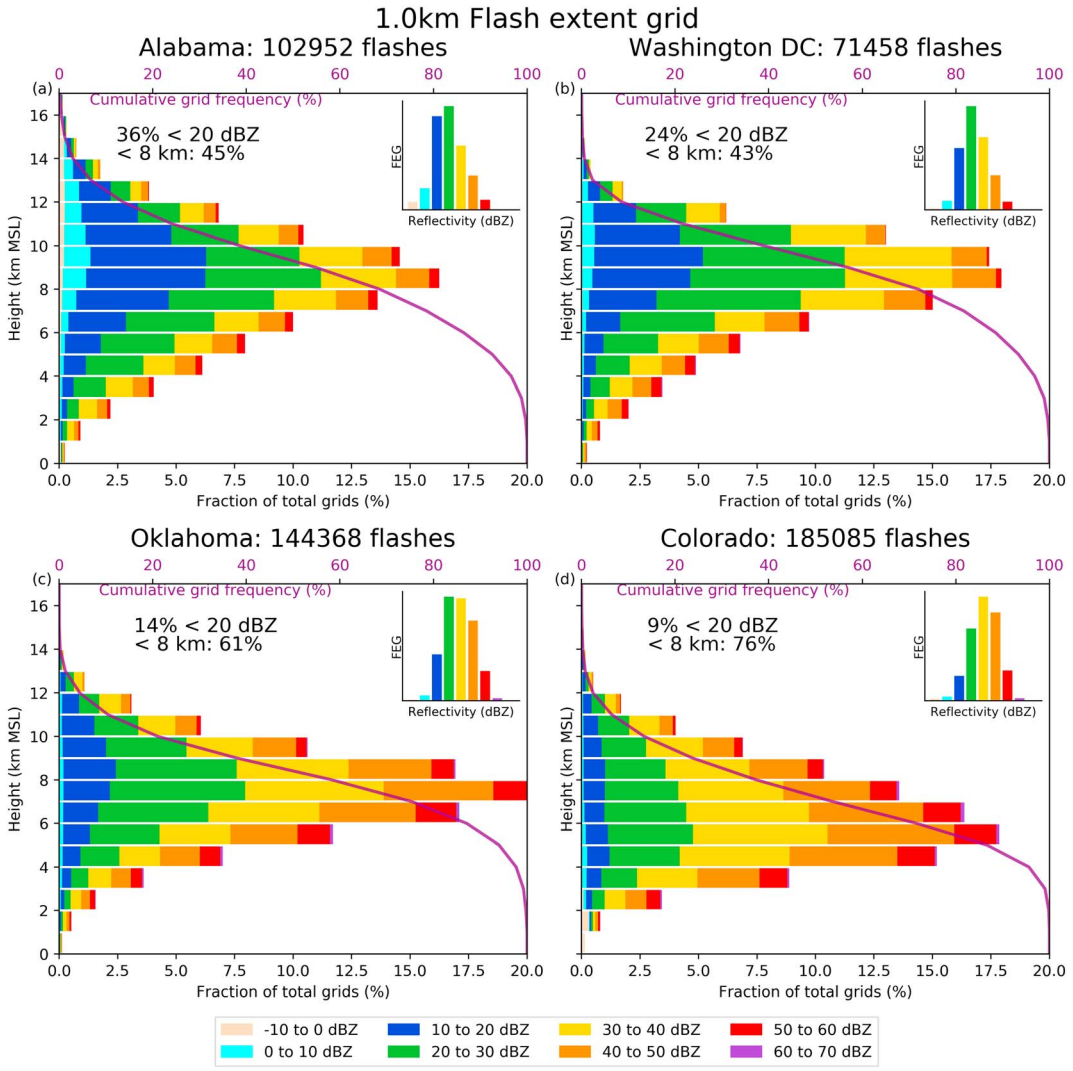

Figure 4. Same as Figure 3 but for flash extent grids (FEGs) calculated on a 1 km grid. MSL = mean sea level.

3.2. Regional Vertical Flash Extent Variability

The altitudes of VHF source and flash extent grids and collocated reflectivity has yielded some interesting results. However, these methods have biases that are inherently tied to the LMA technique itself. We now address this bias by using a different metric to estimate the full vertical extent of flashes. Figure 7 shows a joint histogram of the bottom (measured by the lowest-altitude source in a flash) and top (measured by the highest altitude source in a flash) of every flash in our exhaustive data set. Figure 8 shows the distributions of the minimum, mean, and maximum VHF source altitude, as well as the difference between the maximum and minimum sources for all flashes in each region. These values are output directly by the flash clustering algorithm and do not require gridding of any kind, in contrast with our previous results.

The average minimum flash altitude for all flashes in AL is 9 km MSL, the average mean flash altitude is close to 10 km MSL, and the average maximum flash altitude is 11.5 km MSL (Figures 7 and 8). The distributions of flash metrics in D.C. resemble AL, with a systematic downward shift of approximately 1.0 km. Each flash metric in OK is shifted lower than D.C. by approximately 0.5 km. This analysis reveals some interesting behaviors in the CO flashes. Two separate maxima are apparent in the joint distribution in Figure 7, which can be seen in Figure 8 as well. The mode of minimum flash altitudes in CO is around 4.5 km MSL, while a shoulder is present at approximately 9 km MSL. A similar signal is observed from the mean and maximum flash altitudes. The means of each flash height parameter distribution in Figure 8 are all approximately 2.0 km lower than

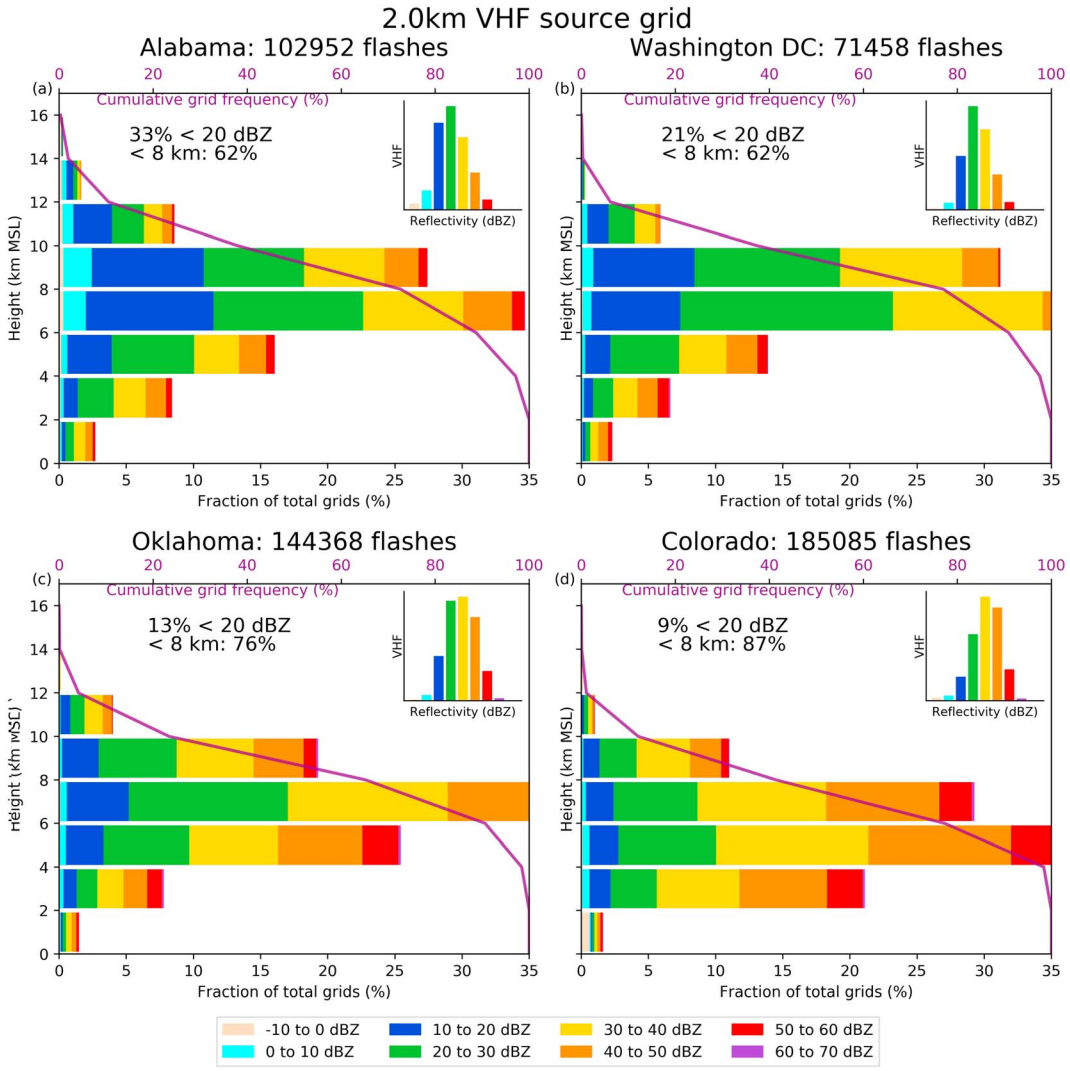

Figure 5. Same as Figure 3 but for very high frequency (VHF) sources on a 2 km grid. MSL = mean sea level.

corresponding values in AL and approximately 0.7 km lower than OK. These values are very similar to the differences between average gridded flash heights (Figures 3–6) as well.

Figure 8d shows the distribution of vertical flash extents (difference between the top and bottom of each flash) for each region. Immediately apparent are the similarities in each region, especially in the frequencies of vertical flash extents larger than ~3 km. The main differences exist in the smaller vertical flash extents. Perhaps the differences in VHF source criteria are manifesting here. The two regions with the 10 VHF source threshold (OK and CO) have lower frequencies of vertical flash extents less than 1 km while the two regions that have a 2 VHF source threshold (AL and D.C.) have higher frequencies of vertical flash extents less than 1 km. However, these differences are only 5–10% of the entire data set. Moreover, AL has the highest average vertical flash extent of all the regions (2.8 km), even though it has the 2 VHF source threshold. Furthermore, the averages for each region are within 0.5 km of each other. These results suggest that the vertical flash extent metric is relatively insensitive to LMA detection capabilities, assuming the characteristics of the physical flashes in each region are not significantly different.

3.3. Charge Structure Dependence

The propensity for anomalous charge structures (Fuchs et al., 2015), lower flash initiation altitudes (Fuchs et al., 2016), and flash extent (this study) in Colorado provide some evidence that the storm-integrated

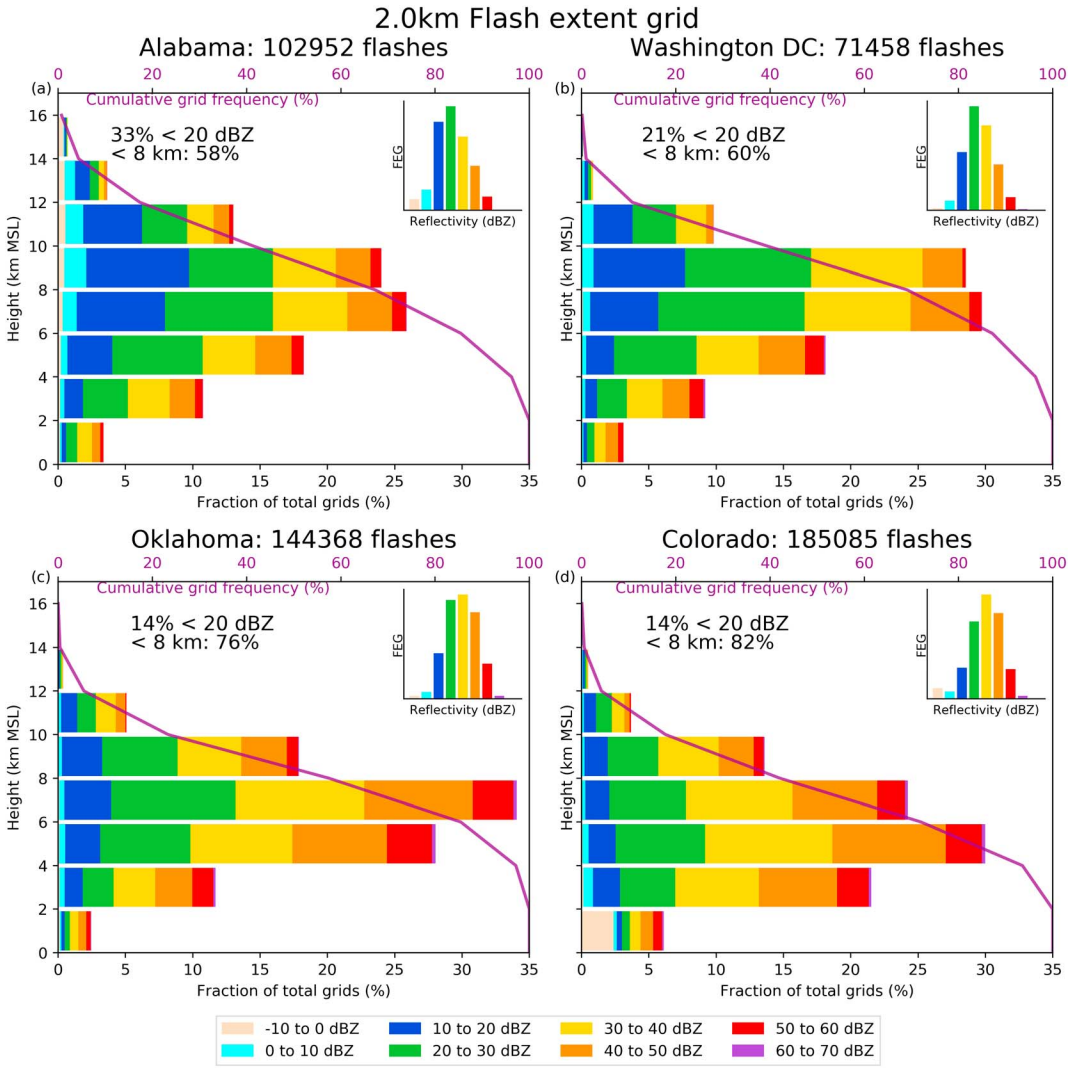

Figure 6. Same as Figure 3 but for flash extent grids (FEGs) calculated on a 2 km grid. MSL = mean sea level.

lightning flash locations are controlled to first order by macroscale charge structure. To investigate this claim more directly, Figure 9 shows a joint distribution of flash bottom and flash top (measured by the same method as Figure 7), partitioned by the LMA mode temperature of the storm in which each flash occurred, with all regions combined. This is made possible by the fact that the distributions of vertical flash extent are very similar for each region (Figure 8d). Normal polarity charge structures are usually characterized by LMA mode temperatures (proxy for dominant positive charge) < -30°C, while anomalous charge structures are usually characterized by LMA mode temperatures > -30°C (Lang & Rutledge, 2011; Wiens et al., 2005).

Figure 9a shows the flash top and bottom for all flashes that occurred in storms with an LMA mode between -60°C and -40°C. Most flashes in these storms have bottom heights of ~9 km MSL or higher, and most top heights are ~11 km MSL or higher. Fuchs et al. (2015) showed that storms with very cold LMA modes are typically quite intense and are argued to have positively charged ice crystals at significant heights as a result of strong updrafts. For lightning flashes that occurred in normal polarity storms with LMA mode temperatures between -40°C and -30°C, the average altitude of flash bottoms was 8 km MSL and the average altitude of flash tops was ~10 km MSL. Notice that both heights are lower than flashes from Figure 8a, possibly due to the lower altitude (higher temperature) of the strong positive charge, as inferred by the LMA. Fuchs et al. (2015) showed that these storms had lower flash rates than storms with LMA mode temperatures < -40°C and therefore were not as intense. Figure 9c shows the top and bottom of all flashes in storms with LMA

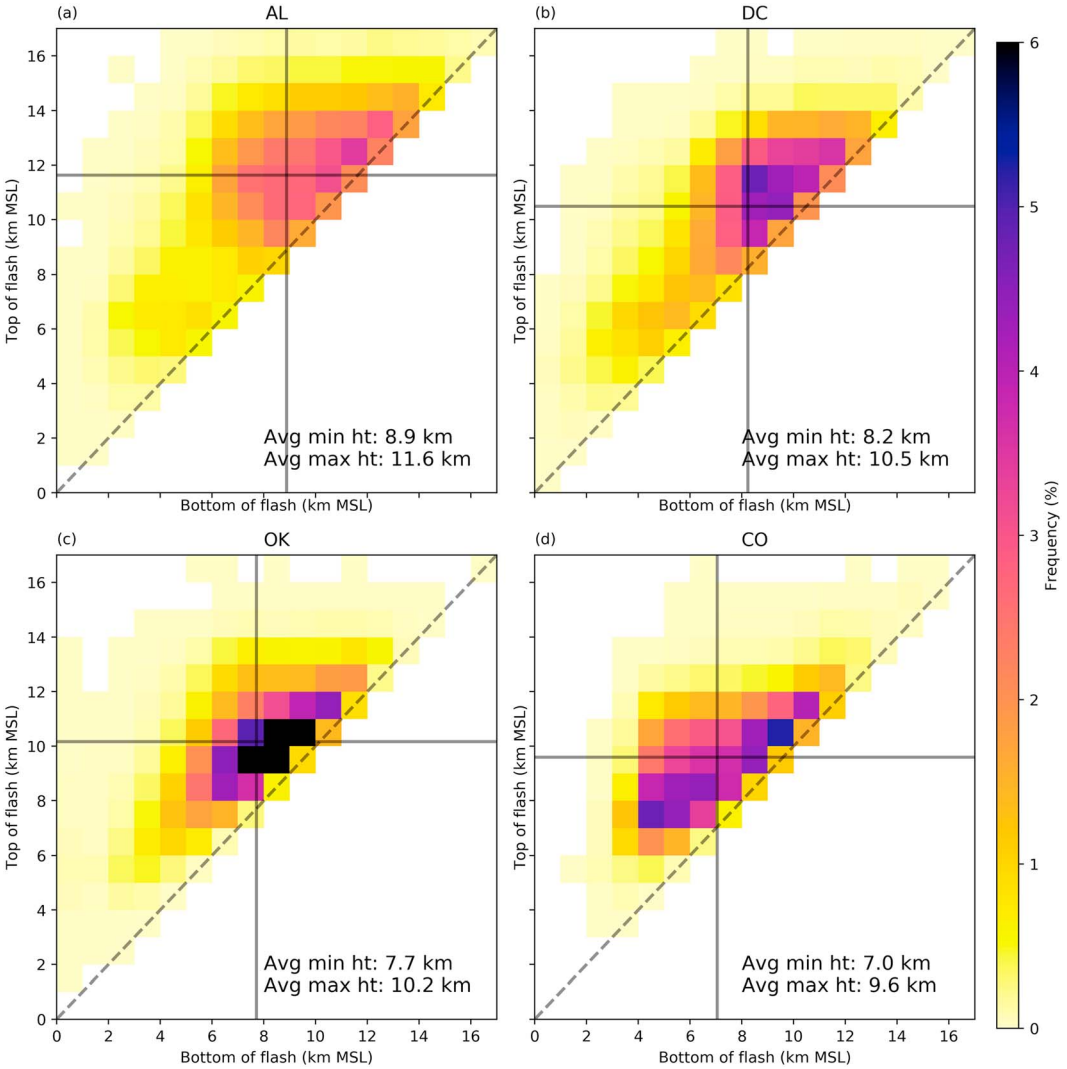

Figure 7. Joint histogram of the bottom (as measured by the lowest-altitude Lightning Mapping Array very high frequency source) and the top (as measured by the highest altitude Lightning Mapping Array very high frequency source) of each flash in (a) Alabama, (b) Washington, D.C., (c) Oklahoma, and (d) Colorado gridded to 1 km. The average flash top and bottom are indicated in text on the bottom right of each panel and graphically (black lines). MSL = mean sea level.

mode temperatures between −30°C and −15°C, which are typically thought of as possessing anomalous polarity charge structures (strong midlevel positive charge). The downward shift in both flash bottom and flash top is evident, as the average value of the bottom of flashes is 7.1 km MSL while the average top height is 9.6 km MSL. This downward shift is likely due to the presence of a region of strong positive charge at warmer temperatures in anomalous storms. Finally, the joint distribution of all flashes that occurred in storms with LMA mode temperatures between −15°C and 0°C is shown in Figure 9d. These flashes are the lowest of all storm categories, with an average value of 6.0 km MSL for the bottom of flashes and an average top altitude of 8.7 km MSL.

There is substantial regional disparity in lightning production as a function of charge structure. For example, 84% of the flashes in the AL region were produced by normal polarity storms (as defined earlier). In contrast, only 29% of the flashes in the CO were produced by normal polarity storms while 69% of the flashes were produced by anomalous polarity storms. It appears that the prevalence of anomalous storms in Colorado is largely responsible for the lower altitude flashes in the region. Note that the percentages of flashes in each region do not add to exactly 100%; this is because a very small percentage of flashes occurred in storms with LMA mode temperatures colder than −60°C or warmer than 0°C.

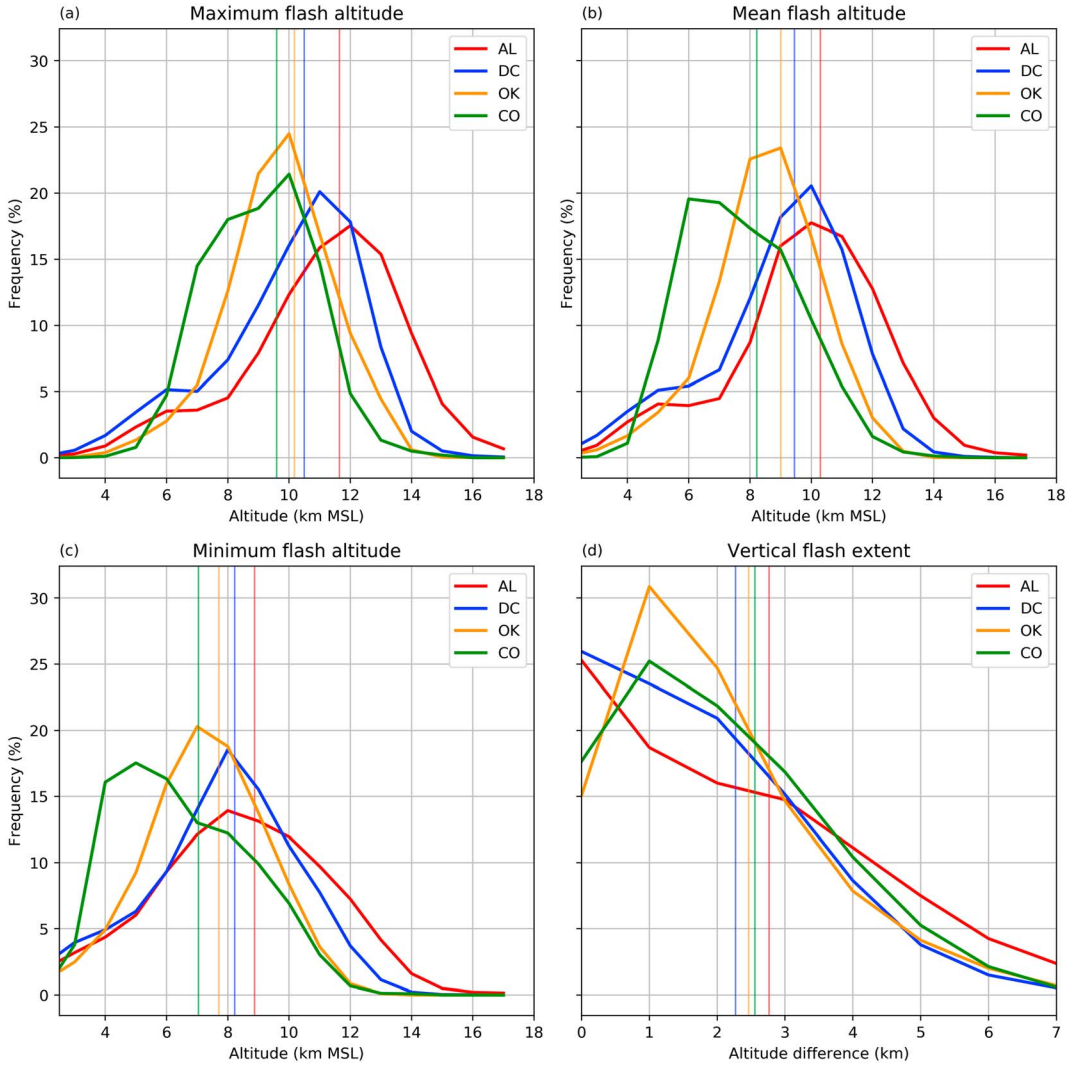

Figure 8. Histograms of (a) minimum flash altitude, (b) mean flash altitude, (c) maximum flash altitude, and (d) the vertical flash extent (difference between maximum and minimum) for each region gridded to 1 km (colors follow the legend). The vertical lines show the average values for each region using the same colors. MSL = mean sea level.

4. Summary and Discussion

VHF-based mapping of over 500,000 lightning flashes by LMAs from over 4,000 storms in diverse environments demonstrated the variability of lightning flash locations with respect to collocated radar reflectivity and height, which resulted in some consequential insights. We used three (somewhat independent) methods to investigate the variability of lightning flash locations, each of which had different sensitivities to the inherent bias of LMAs to negative breakdown into positive charge. Regardless of the particular sensitivities, each of those analysis methods resulted in the same conclusions.

Colorado storms produced flashes at the lowest altitudes and strongest collocated reflectivities, using each analysis method in this study. This was attributed to the prevalence of anomalous storms in the Colorado region, which corroborates the claims made by Fuchs et al. (2016). Indeed, the flashes that initiate at lower altitudes in Colorado translate to lightning distributions centered lower in the storm, implying that flashes that start low tend to stay low in these storms. Conversely, flashes in Alabama and D.C. storms occurred at high altitudes and in regions of lower reflectivity, which was attributed to the prevalence of normal polarity storms in those regions. The vertical lightning distributions in Oklahoma storms fell between Alabama/D.C. and Colorado, which is consistent with the increased lightning production from anomalous storms in Oklahoma compared to the Alabama and D.C. regions (Fuchs et al., 2015, and this study).

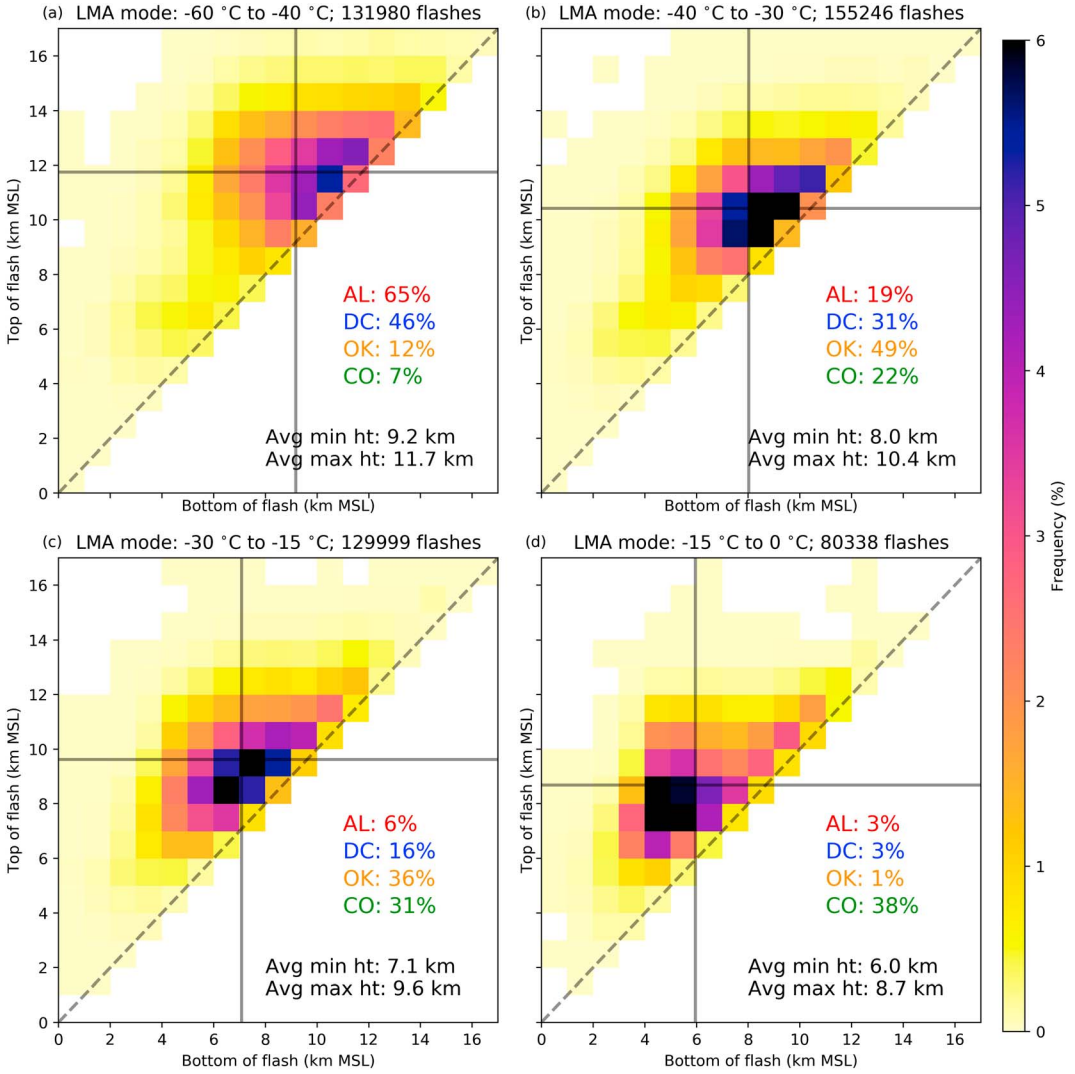

Figure 9. Joint histograms of the bottom and top of each flash for (a) Lightning Mapping Array (LMA) mode temperatures between −60°C and −40°C, (b) LMA mode temperatures between −40°C and −30°C, (c) LMA mode temperatures between −30°C and −15°C, and (d) LMA mode temperatures between −15°C and 0°C gridded to 1 km. Average flash minimum and maximum heights and percentage of total flashes from each region are indicated in each panel in addition to the percentage of the total flashes in each region that were produced by storms in a particular LMA mode temperature range. Note that for each region, the numbers do not add up to exactly 100% because a small fraction of flashes were produced by storms with LMA mode temperatures less than −60°C or greater than 0°C. MSL = mean sea level.

The low-altitude flashes in Colorado anomalous storms may contribute to discrepancies between LMA and satellite climatologies in the Colorado region where annual average flash densities and IC:CG values derived from LMA observations are approximately 300% larger than corresponding satellite estimates (Cecil et al., 2014; Fuchs et al., 2016). Much smaller differences between LMA- and satellite-derived lightning estimates were observed in Alabama and D.C., where flash altitudes were considerably higher. Note that the Oklahoma region was not included in the Fuchs et al. (2016) study.

Based on the relationship between storm-scale charge structures and flash altitudes, we surmise that satellite detection efficiencies may be lower in regions where anomalous storms occur. Evidently, the combination of low-altitude flashes and high radar reflectivity reduces the ability of photons to escape through the top of the cloud and be detected by optical detectors on satellites. This is in accordance with other studies that have shown the position of a flash within a cloud affects its optical detection outside of the cloud (Light et al., 2001; Thomas et al., 2000; Thomason & Krider, 1982). Note that the satellite-based estimates of annual flash density for Alabama were based on the Lightning Imaging sensor (Christian et al., 1999), while the estimates

in D.C. and Colorado were based on the Optical Transient Detector (Christian et al., 2003). However, Cecil et al. (2014) and Fuchs et al. (2016) note that the use of these two different detectors are not expected to significantly change the annual average flash density estimates.

The relationship between storm-scale charge structure (inferred by the LMA) and flash altitude is quite interesting. Because lightning initiates in strong electric fields and propagates into nearby charge regions, it is perhaps not surprising that anomalous storms have different flash location distributions than normal storms, at least in a broad sense. A majority of flashes in normal polarity storms initiate and propagate between the upper-level positive charge region and the midlevel negative charge region. However, it appears that the charge structures in anomalous storms are not the exact opposite of the charge structures in normal storms. If they were, flashes would initiate and propagate between the upper-level negative charge and the middle- or lower-level positive charge. In this case, lightning would still occur in similar locations, since the electric fields would be the same magnitude but in the opposite direction. The results from this study suggest that this not the case, which demonstrates the need for more research on the details of charge configurations in anomalous storms.

The variability in lightning flash locations with respect to height and collocated reflectivity may have implications for LNO_x transport and conversion to ozone. Anomalous storms in Colorado preferentially produce flashes at lower altitudes, so LNO_x is expected to be produced at lower altitudes in those storms. Because the ozone production efficiency of NO_x is dependent on altitude (e.g., Finney et al., 2016), anomalous storms may have different storm-integrated ozone production efficiency than normal polarity storms. Furthermore, the vertical distribution of LNO_x may result in significant variability in LNO_x advection, and subsequent ozone production efficiency (Lin et al., 1988). Additionally, Colorado storms had the highest percentage of lightning flashes in reflectivities greater than 20 dB*Z*, the metric used to place NO_x in several chemical models. Conversely, more than a third of the lightning flashes in Alabama storms occurred in reflectivities less than 20 dB*Z*. It is unclear what (if any) impact the parameterization placing NO_x within the 20 dB*Z* isopleth, regardless of storm characteristics, may have on the resulting NO_x and ozone distributions in a model. Regardless, all these factors need to be understood in order to fully understand the production of NO_x and ozone by lightning.

Acknowledgments
The authors would like to thank Paul Hein for the general technical assistance. The authors would also like to thank the three reviewers for their comments and multiple suggestions that improved the paper. Rich Blakeslee and Larry Carey provided access to the Alabama and Washington, D.C., LMA data. Don MacGorman provided LMA data from the Oklahoma region. The LMA networks, data, and processing are managed by Paul Krehbiel, William Rison, and Ronald Thomas at New Mexico Tech. Visit https://github.com/deeplycloudy/lmatools for more information about the flash clustering algorithm used in this database. Inquiries and any additional information regarding the study or data used can be directed to the corresponding author (brfuchs@atmos.colostate.edu). Funding for this study is provided by the NSF PDM grant AGS-1429925 and NOAA grant NA14OAR4320125.

References

Boccippio, D., Cummins, K. L., Christian, H. J., & Goodman, S. J. (2001). Combined satellite and surface-based estimation of the intracloud-cloud-to-ground lightning ratio over the continental United States. *Monthly Weather Review*, *129*(1), 108–122. https://doi.org/10.1175/1520-0493(2001)129%3C0108:CSASBE%3E2.0.CO;2

Bruning, E., Weiss, S. A., & Calhoun, K. M. (2014). Continuous variability in thunderstorm primary electrification and an evaluation of inverted-polarity terminology. *Atmospheric Research*, *135*, 274–284.

Bruning, E. C. (2013). Streamed clustering of lightning mapping data in Python using sklearn, in Scientific Computing With Python, vol. 2.

Bruning, E. C., Rust, W. D., Schuur, T. J., MacGorman, D. R., Krehbiel, P. R., & Rison, W. (2007). Electrical and polarimetric radar observations of a multicell storm in TELEX. *Monthly Weather Review*, *135*(7), 2525–2544. https://doi.org/10.1175/MWR3421.1

Cecil, D. J., Buechler, D. E., & Blakeslee, R. J. (2014). Gridded lightning climatology from TRMM-LIS and OTD: Dataset description. *Atmospheric Research*, *135*, 404–414.

Chmielewski, V. C., & Bruning, E. C. (2016). Lightning Mapping Array flash detection performance with variable receiver thresholds. *Journal of Geophysical Research: Atmospheres*, *121*, 8600–8614. https://doi.org/10.1002/2016JD025159

Christian, H. J., Blakeslee, R. J., Goodman, S. J., Boccippio, D., Boeck, W. L., Buechler, D. E., et al. (2003). Global frequency and distribution of lightning as observed from space by the Optical Transient Detector. *Journal of Geophysical Research*, *108*, 4005. https://doi.org/10.1029/2002JD002347

Christian, H. J., Blakeslee, R. J., Goodman, S. J., Mach, D. A., Stewart, M. F., Buechler, D. E., et al. (1999). The lightning imaging sensor. *NASA Conference Publication*, *1*, 746–749.

Coleman, L., Marshall, T., Stolzenburg, M., Hamlin, T., Krehbiel, P., Rison, W., & Thomas, R. (2003). Effects of charge and electrostatic potential on lightning propagation. *Journal of Geophysical Research*, *108*(D9), 4298. https://doi.org/10.1029/2002JD002718

DeCaria, A. J., Pickering, K. E., Stenchikov, G. L., & Ott, L. E. (2005). Lightning-generated NOx and its impact on tropospheric ozone production: A three-dimensional modeling study of a Stratosphere-Troposphere Experiment: Radiation, Aerosols and Ozone (STERAO-A) thunderstorm. *Journal of Geophysical Research*, *110*, D14303. https://doi.org/10.1029/2004JD005556

DeCaria, A. J., Pickering, K. E., Stenchikov, G. L., Scala, J. R., Stith, J. L., Dye, J. E., et al. (2000). A cloud-scale model study of lightning-generated NO_x in an individual thunderstorm during STERAO-A. *Journal of Geophysical Research*, *105*, 11,601–11,616. https://doi.org/10.1029/2000JD900033

Finney, D. L., Doherty, R. M., Wild, O., Young, P. J., & Butler, A. (2016). Response of lightning NO_x emissions and ozone production to climate change: Insights from the Atmospheric Chemistry and Climate Model Intercomparison Project. *Geophysical Research Letters*, *43*, 5492–5500. https://doi.org/10.1002/2016GL068825,%202016GL068825

Fuchs, B. R., Bruning, E. C., Rutledge, S. A., Carey, L. D., Krehbiel, P. R., & Rison, W. (2016). Climatological analyses of LMA data with an open-source lightning flash-clustering algorithm. *Journal of Geophysical Research: Atmospheres*, *121*, 8625–8648. https://doi.org/10.1002/2015JD024663

Fuchs, B. R., Rutledge, S. A., Bruning, E. C., Pierce, J. R., Kodros, J. K., Lang, T. J., et al. (2015). Environmental controls on storm intensity and charge structure in multiple regions of the continental United States. *Journal of Geophysical Research: Atmospheres*, *120*, 6575–6596. https://doi.org/10.1002/2015JD023271

Fuchs, B. R., Rutledge, S. A., Dolan, B., Carey, L. D., & Schultz, C. (2018). Microphysical and kinematic processes associated with anomalous charge structures in isolated convection. *Journal of Geophysical Research: Atmospheres*, *123*. https://doi.org/10.1029/2017JD027540

Goldenbaum, G., & Dickerson, R. (1993). Nitric oxide production by lightning discharges. *Journal of Geophysical Research*, *98*(D10), 18,333–18,338. https://doi.org/10.1029/93JD01018

Huntrieser, H., Schlager, H., Feigl, C., & Höller, H. (1998). Transport and production of NO_x in electrified thunderstorms: Survey of previous studies and new observations at midlatitudes. *Journal of Geophysical Research*, *103*(D21), 28,247–28,264.

Jayaratne, E. R., Saunders, C. P. R., & Hallett, J. (1983). Laboratory studies of the charging of soft-hail during ice crystal interactions. *Quarterly Journal of the Royal Meteorological Society*, *109*(461), 609–630. https://doi.org/10.1002/qj.49710946111

Koshak, W., Solakiewicz, R., Blakeslee, R., Goodman, S., Christian, H., Hall, J., et al. (2004). North Alabama Lightning Mapping Array (LMA): VHF source retrieval algorithm and error analyses. *Journal of Atmospheric and Oceanic Technology*, *21*(4), 543–558. https://doi.org/10.1175/1520-0426(2004)021%3C0543:NALMAL%3E2.0.CO;2

Krehbiel, P. (1986). *The electrical structure of thunderstorms*. Washington, DC: National Academies Press.

Krehbiel, P., Thomas, R. J., Rison, W., Hamlin, T., Davis, M., & Harlin, J. (2000). Lightning mapping observations in central Oklahoma. *Eos*, *81*(3), 21–25. https://doi.org/10.1029/00EO00014

Krehbiel, P. R., Brook, M., & McCrory, R. A. (1979). An analysis of the charge structure of lightning discharges to ground. *Journal of Geophysical Research*, *84*(C5), 2432–2456. https://doi.org/10.1029/JC084iC05p02432

Lang, T. J., & Rutledge, S. A. (2011). A framework for the statistical analysis of large radar and lightning datasets: Results from STEPS 2000. *Monthly Weather Review*, *139*(8), 2536–2551. https://doi.org/10.1175/MWR-D-10-05000.1

Lang, T. J., Rutledge, S. A., Dye, J. E., Venticinque, M., Laroche, P., & Defer, E. (2000). Anomalously low negative cloud-to-ground lightning flash rates in intense convective storms observed during STERAO-A. *Monthly Weather Review*, *128*(1), 160–173. https://doi.org/10.1175/1520-0493(2000)128%3C0160:ALNCTG%3E2.0.CO;2

Light, T., Suszcynsky, D., Kirkland, M., & Jacobson, A. (2001). Simulations of lightning optical waveforms as seen through clouds by satellites. *Journal of Geophysical Research*, *106*(D15), 17,103–17,114. https://doi.org/10.1029/2001JD900051

Lin, X., Trainer, M., & Liu, S. (1988). On the nonlinearity of the tropospheric ozone production. *Journal of Geophysical Research*, *93*(D12), 15,879–15,888. https://doi.org/10.1029/JD093iD12p15879

MacGorman, D. R., Rust, W. D., Krehbiel, P., Rison, W., Bruning, E., & Wiens, K. (2005). The electrical structure of two supercell storms during STEPS. *Monthly Weather Review*, *133*(9), 2583–2607. https://doi.org/10.1175/MWR2994.1

MacGorman, D. R., Straka, J. M., & Ziegler, C. L. (2001). A lightning parameterization for numerical cloud models. *Journal of Applied Meteorology*, *40*(3), 459–478. https://doi.org/10.1175/1520-0450(2001)040%3C0459:ALPFNC%3E2.0.CO;2

Maggio, C., Coleman, L., Marshall, T., Stolzenburg, M., Stanley, M., Hamlin, T., et al. (2005). Lightning-initiation locations as a remote sensing tool of large thunderstorm electric field vectors. *Journal of Atmospheric and Oceanic Technology*, *22*(7), 1059–1068. https://doi.org/10.1175/JTECH1750.1

Mansell, E. R. (2014). Storm-scale ensemble Kalman filter assimilation of total lightning flash-extent data. *Monthly Weather Review*, *142*(10), 3683–3695. https://doi.org/10.1175/MWR-D-14-00061.1

McCaul, E. W., Goodman, S. J., LaCasse, K. M., & Cecil, D. J. (2009). Forecasting lightning threat using cloud-resolving model simulations. *Weather and Forecasting*, *24*(3), 709–729. https://doi.org/10.1175/2008WAF2222152.1

Ott, L. E., Pickering, K. E., Stenchikov, G. L., Allen, D. J., DeCaria, A. J., Ridley, B., et al. (2010). Production of lightning NO_x and its vertical distribution calculated from three-dimensional cloud-scale chemical transport model simulations. *Journal of Geophysical Research*, *115*, D04301. https://doi.org/10.1029/2009JD011880

Pickering, K. E., Wang, Y., Tao, W.-K., Price, C., & Müller, J.-F. (1998). Vertical distributions of lightning NO_x for use in regional and global chemical transport models. *Journal of Geophysical Research*, *103*(D23), 31,203–31,216.

Price, C., Penner, J., & Prather, M. (1997). NO_x from lightning: 1. Global distribution based on lightning physics. *Journal of Geophysical Research*, *102*(D5), 5929–5941. https://doi.org/10.1029/96JD03504

Rison, W., Thomas, R., Krehbiel, P., Hamlin, T., & Harlin, J. (1999). A GPS-based three-dimensional lightning mapping system: Initial observations in central New Mexico. *Geophysical Research Letters*, *26*(23), 3573–3576. https://doi.org/10.1029/1999GL010856

Rust, W. D., MacGorman, D. R., Bruning, E. C., Weiss, S. A., Krehbiel, P. R., Thomas, R. J., et al. (2005). Inverted-polarity electrical structures in thunderstorms in the Severe Thunderstorm Electrification and Precipitation Study (STEPS). *Atmospheric Research*, *76*(1-4), 247–271. https://doi.org/10.1016/j.atmosres.2004.11.029

Saunders, C. P. R., Keith, W. D., & Mitzeva, R. P. (1991). The effect of liquid water on thunderstorm charging. *Journal of Geophysical Research*, *96*(D6), 11,007–11,017. https://doi.org/10.1029/91JD00970

Saunders, C. P. R., & Peck, S. L. (1998). Laboratory studies of the influence of the rime accretion rate on charge transfer during graupel/crystal collisions. *Journal of Geophysical Research*, *103*(D12), 13,949–13,956. https://doi.org/10.1029/97JD02644

Schumann, U., & Huntrieser, H. (2007). The global lightning-induced nitrogen oxides source. *Atmospheric Chemistry and Physics*, *7*(14), 3823–3907. https://doi.org/10.5194/acp-7-3823-2007

Takahashi, H., Suzuki, K., & Stephens, G. (2017). Land-ocean differences in the warm-rain formation process in satellite and ground-based observations and model simulations. *Quarterly Journal of the Royal Meteorological Society*, *143*(705), 1804–1815. https://doi.org/10.1002/qj.3042

Takahashi, T. (1978). Riming electrification as a charge generation mechanism in thunderstorms. *Atmospheric Sciences*, *35*(8), 1536–1548. https://doi.org/10.1175/1520-0469(1978)035%3C1536:REAACG%3E2.0.CO;2

Tessendorf, S. A., Rutledge, S. A., & Wiens, K. C. (2007). Radar and lightning observations of normal and inverted multicellular storms from STEPS. *Monthly Weather Review*, *135*(11), 3682–3706. https://doi.org/10.1175/2007MWR1954.1

Thomas, R. J., Krehbiel, P. R., Rison, W., Hamlin, T., Boccippio, D. J., Goodman, S. J., & Christian, H. J. (2000). Comparison of ground-based 3-dimensional lightning mapping observations with satellite-based LIS observations in Oklahoma. *Geophysical Research Letters*, *27*(12), 1703–1706. https://doi.org/10.1029/1999GL010845

Thomas, R. J., Krehbiel, P. R., Rison, W., Hamlin, T., Harlin, J., & Shown, D. (2001). Observations of VHF source powers radiated by lightning. *Geophysical Research Letters*, *28*(1), 143–146. https://doi.org/10.1029/2000GL011464

Thomas, R. J., Krehbiel, P. R., Rison, W., Hunyady, S. J., Winn, W. P., Hamlin, T., & Harlin, J. (2004). Accuracy of the lightning mapping array. *Journal of Geophysical Research*, *109*, D14207. https://doi.org/10.1029/2004JD004549

Thomason, L., & Krider, E. (1982). The effects of clouds on the light produced by lightning. *Journal of the Atmospheric Sciences*, *39*(9), 2051–2065. https://doi.org/10.1175/1520-0469(1982)039%3C2051:TEOCOT%3E2.0.CO;2

Wiens, K. C., Rutledge, S. A., & Tessendorf, S. A. (2005). The 29 June 2000 supercell observed during STEPS. Part II: Lightning and charge structure. *Journal of Atmospheric Research*, *62*(12), 4151–4177. https://doi.org/10.1175/JAS3615.1

Williams, E. R. (1985). Large-scale separation in thunderclouds. *Journal of Geophysical Research*, *90*(D4), 6013–6025. https://doi.org/10.1029/JD090iD04p06013

Williams, E. R. (1989). The tripole structure of thunderstorms. *Journal of Geophysical Research*, *94*(D11), 13,151–13,167. https://doi.org/10.1029/JD094iD11p13151

Williams, E. R., Mushtak, V., Rosenfeld, D., Goodman, S., & Boccippio, D. (2005). Thermodynamic conditions that lead to superlative updrafts and mixed-phase microphysics. *Atmospheric Research*, *76*(1-4), 288–306. https://doi.org/10.1016/j.atmosres.2004.11.009

Workman, E. J., & Reynolds, S. E. (1950). Electrical phenomena occurring during the freezing of dilute aqueous solutions and their possible relationship to thunderstorm electricity. *Physics Review*, *78*(3), 254–259. https://doi.org/10.1103/PhysRev.78.254

Yuter, S. E., & Houze, R. A. (1998). The natural variability of precipitating clouds over the Western Pacific warm pool. *Quarterly Journal of the Royal Meteorological Society*, *124*(545), 53–99. https://doi.org/10.1002/qj.49712454504

Zhang, J., Howard, K., Langston, C., Vasiloff, S., Kaney, B., Arthur, A., et al. (2011). National Mosaic and Multi-Sensor QPE (NMQ) system: Description, results, and future plans. *Bulletin of the American Meteorological Society*, *92*(10), 1321–1338. https://doi.org/10.1175/2011BAMS-D-11-00047.1